Assessing the Uncertainties in Ozone and SOA Predictions due to Different Branching Ratios of the Cresol Pathway in the Toluene-OH Oxidation Mechanism

Jie Zhang[1], Minsu Choi[1], Yuemeng Ji[2], Renyi Zhang[3], Ruiqin Zhang[4,5], Qi Ying[1,*]

[1] Zachry Department of Civil and Environmental Engineering, Texas A&M University, College Station, TX 77843, USA

[2] School of Environmental Science and Engineering, Guangdong University of Technology, Guangzhou, 510006, China.

[3] Department of Atmospheric Sciences, Texas A&M University, College Station, TX 77843, USA

[4] College of Chemistry, Zhengzhou University, Zhengzhou, 450001, China.

[5] School of Ecology and Environment, Zhengzhou University, Zhengzhou, 450001, China

Supplementary Information

[*] Corresponding Author: Q. Ying (qying@civil.tamu.edu). Phone: 979-845-9709.

Table S1 Initial conditions of the toluene oxidation chamber experiments simulated in this study

Experiments[^]	Toluene (ppb)	NO_x (ppb)	H_2O_2 (ppm)	OH (10^6 cm^3)	Seed[#] (μg m^{-3})	T (^oC)	Lights
H-1	940	1300	49	3.1	61	20	30%
H-2	380	720	72	3.5	64	20	100%
H-3	950	570	91	2.6	113	20	100%
H-4	190	320	87	1.9	50	18	100%
H-5	180	270	57	1.1	42	12	100%
H-6	200	430	85	2.4	36	31	100%
L-1	380	<5[$]	88	1.6	59	20	100%
L-2	270	<5	40	1	57	11	100%
L-3	180	<5	46	0.6	45	11	100%
L-4	200	<5	42	1.2	60	32	100%
L-5	570	<5	87	1.4	61	21	100%
L-6	570	<5	45	1.6	47	21	100%

[^] H-1 to H-6 are high-NO_x experiments, and L1 to L6 are low-NO_x experiments.

[*] Experiment H-1 was conducted with ~30% of the blacklights and the optimal J_{NO2} was scaled accordingly to verify the MCM mechanism. The SOA mass yields at C_{OM} = 10 and 20 μg m^{-3} with the new mechanism (0.04 and 0.07) were slightly higher than those from the original mechanism (0.03 and 0.06), and both are slightly lower than the measured yields in Hildebrandt et al.'s study (0.08 and 0.12). This experiment was not included in the simulations to estimate J_{NO2} or in the 2-product parameter fitting.

[$] Use 3 ppb in the model simulations

[#] included in the model as $(NH_4)_2SO_4$.

Table S2 Mean fractional bias and mean fraction error of predicted hourly $PM_{2.5}$ at 5 United States Consulates in China in January and July 2013

		January			July	
Site	No. of data	MFB*	MFE*	No. of data	MFB	MFE
Beijing	611	-0.528	0.641	609	-0.545	0.688
Shanghai	596	-0.564	0.611	593	-0.255	0.455
Guangzhou	613	-0.310	0.484	556	-0.298	0.565
Chengdu	606	-0.158	0.408	592	0.061	0.439
Shenyang	-	-	-	514	0.054	0.605

*MFE: Mean fractional bias. $MFE = \frac{2}{N}\sum\left|\frac{O_i - P_i}{O_i + P_i}\right|$. MFB: Mean fractional bias. $MFB = \frac{2}{N}\sum\left(\frac{O_i - P_i}{O_i + P_i}\right)$. P and O represent predictions and observations, respectively.

Table S3 2p model parameters for ARO1 SOA yield under high-NOx and low-NOx conditions used in this study

		Parameters Case C0, C2	Case C1
High-NO_x conditions	α_1	0.239	0.770
	C_1^* (μg m^{-3})	10.15	21.10
	α_2	0.738	-
	C_2^* (μg m^{-3})	2147	-
Low-NO_x conditions	α_1	0.100	0.179
	C_1^* (μg m^{-3})	9.592	-

Table S4 Observed average concentrations of major aromatic compounds in Chinese cities. Units are ppb.

City	Toluene	Ethylbenzene	Xylenes	TEX*	Time	Reference
Beijing (u[#])	2.42	0.79	1.24	4.44	Nov. 2014	[1]
Beijing (s)	0.92	0.37	0.46	1.75		
Beijing(s)	0.82	0.20	0.75	1.77	Nov.2017-Feb. 2018	
Chengdu (u)	1.80	0.83	1.71	4.34	Oct.2016 – Sep.2017	[2]
Shanghai (u)	11.10	3.76	4.98	19.84	Nov. 2013 (Non-H^)	[3]
	14.20	5.23	8.23	27.66	Nov. 2013 (H)	
Guangzhou (u)	4.64	0.79	0.74	6.17	Nov.-Dec. 2009	[4]
Guangzhou (s)	2.97	0.57	0.58	4.11		
Nanjing (s)	1.67	1.01	1.05	3.73	Sep. 2011-Feb.2012	[5]
Nanjing (s)	3.23	1.21	1.86	6.30	Aug. 2013	[6]
Guangzhou (u)	5.45	1.31	3.27	10.03	Jan. 2017 (daytime)	[7]
	6.08	1.81	5.52	13.41	Jan. 2017 (nighttime)	
Zhengzhou (u)	1.12	0.31	1.27	2.70	Jul.-Sep. 2019	Unpublished

* Sum of toluene, ethylbenzene and xylenes (o + m/p). These are the major compounds included in the SAPRC model species ARO1 (toluene+ethylbenzene) and ARO2 (xylenes).

^ Non-H stands for non-hazy days, and H stands for hazy days.

[#] (u) stands for urban monitor sites, and (s) stands for suburban monitor sites.

Table S5 Predicted concentrations of ARO1 and ARO2 concentrations from the base case simulation. Units are ppb.

	January			July		
Site	ARO1	ARO2	Sum	ARO1	ARO2	Sum
Beijing	4.12 (1.23,10.02)	2.67 (0.69,6.87)	6.79 (1.92,16.88)	1.63 (0.45,4.58)	0.87 (0.21,2.77)	2.49 (0.67,7.35)
Shenyang	3.54 (1.96,7.94)	1.84 (1.04,4.22)	5.39 (3.01,12.15)	1.63 (0.81,3.85)	0.80 (0.39,1.97)	2.44 (1.20,5.82)
Nanjing	4.32 (3.15,6.49)	2.19 (1.53,3.38)	6.52 (4.67,9.86)	1.39 (0.94,3.76)	0.70 (0.47,1.92)	2.09 (1.42,5.68)
Chengdu	3.99 (1.10,6.16)	2.25 (0.34,3.59)	6.24 (1.44,9.75)	2.67 (0.32,4.52)	1.38 (0.11,2.43)	4.05 (0.43,6.96)
Guangzhou	3.92 (1.44,3.92)	1.77 (0.51,1.82)	5.69 (1.95,5.73)	2.88 (0.29,3.34)	1.36 (0.14,1.72)	4.24 (0.43,5.07)
Shanghai	2.79 (2.59,5.00)	1.38 (1.12,2.65)	4.18 (3.71,7.64)	2.03 (1.54,3.40)	0.92 (0.68,1.66)	2.96 (2.22,5.05)
Zhengzhou	4.67 (3.21,4.67)	2.43 (1.54,2.43)	7.10 (4.75,7.10)	2.00 (0.92,2.00)	1.00 (0.42,1.00)	3.00 (1.34,3.00)

Note: For each city the concentrations are from the grid cell where the urban center is located. The numbers in the parenthesis represent the minimum and maximum concentrations with the 9 grid cells with the urban center grid cell in the middle.

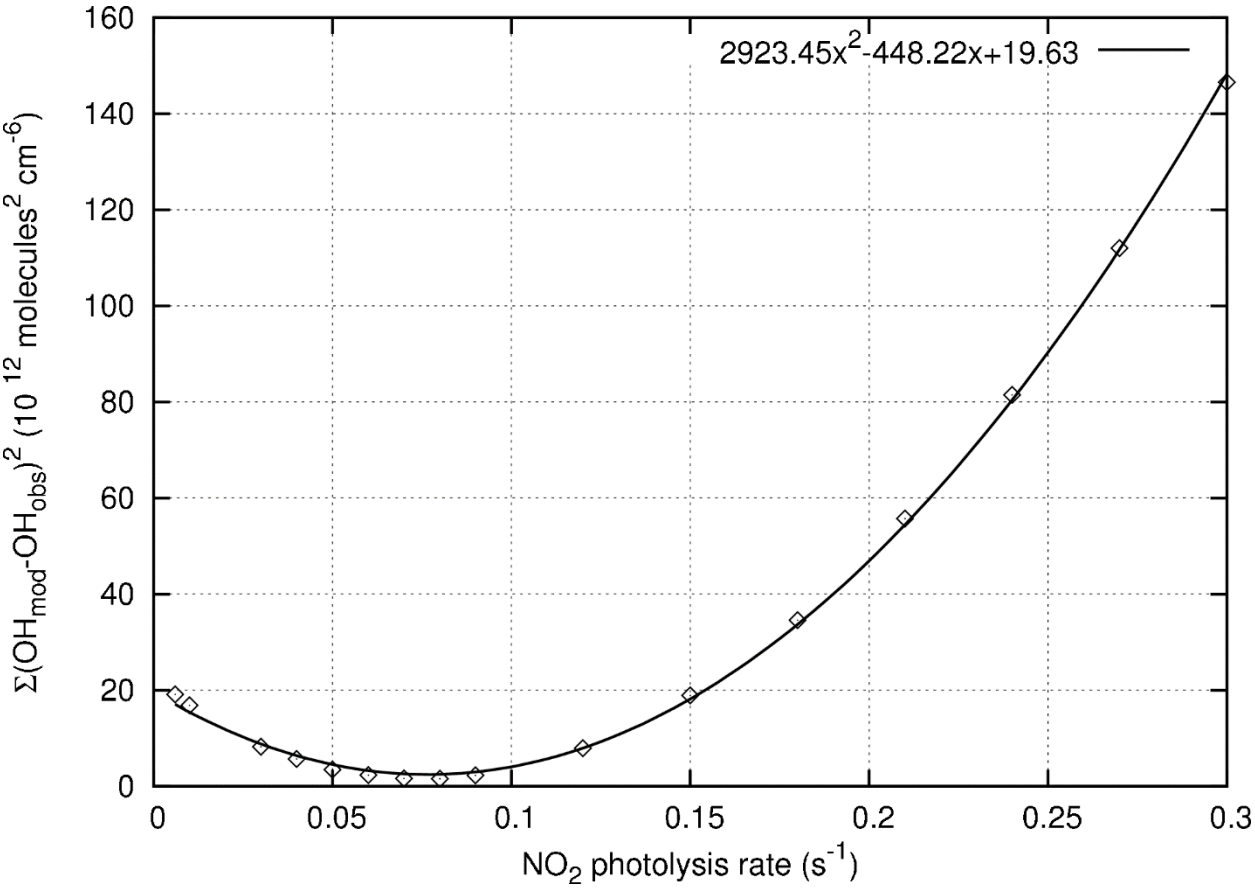

Figure S1. The sum of squared errors (SSE) (units: 10^{12} molecules cm^{-3}) of predicted OH for the high-NO_x chamber experiments with different NO_2 photolysis rate coefficients (J_{NO2}). A quadratic function was used to fit the SSE as a function of j_{NO2}. The minimum SSE occurs at J_{NO2}=0.0767 min^{-1}.

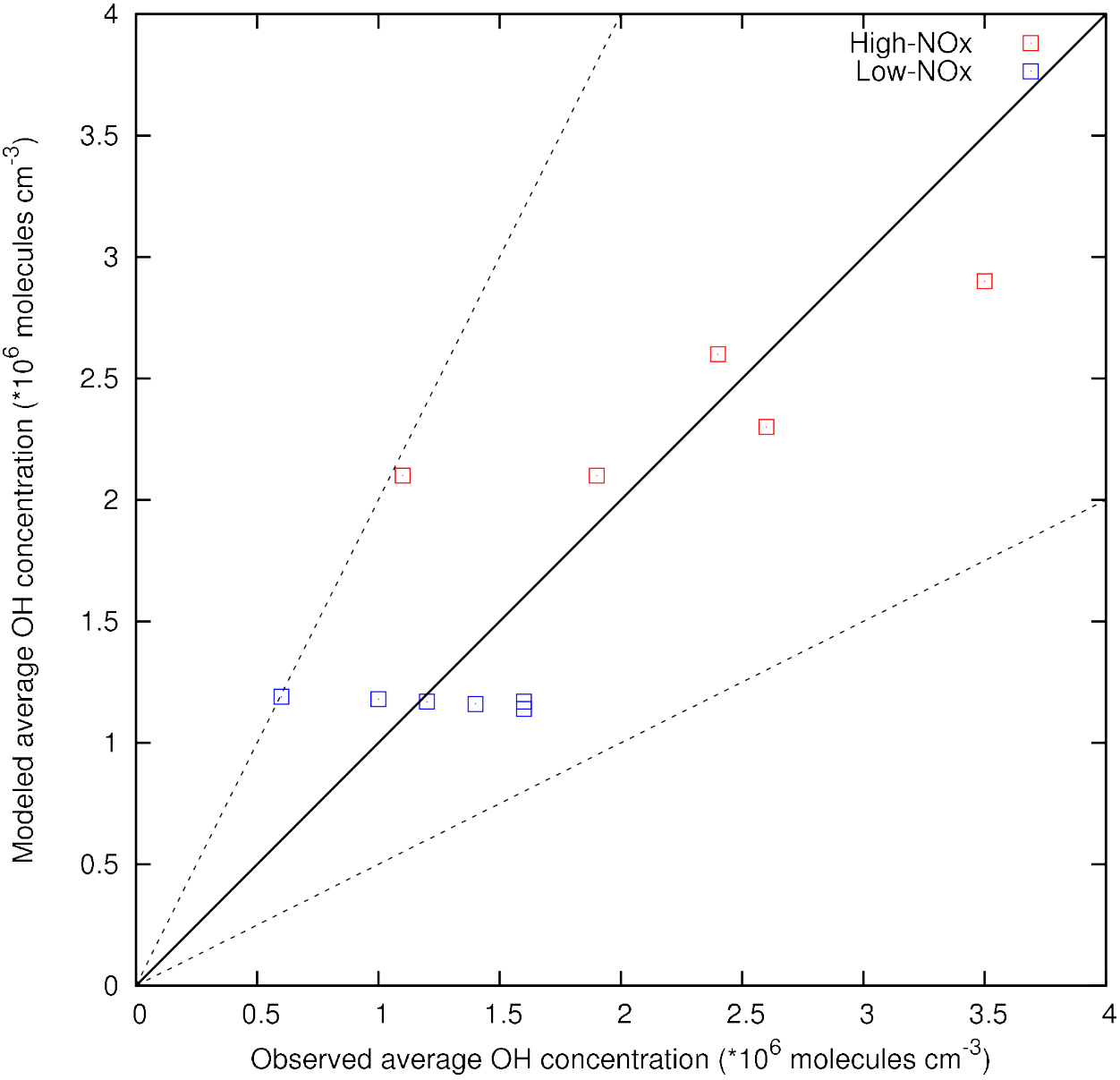

Figure S2. Predicted and reported OH for all chamber experiments simulated in this study with the optimal photolysis rate coefficient (J_{NO2}) of 0.0767 min^{-1}. The optimized J_{NO2} was found based on simulations for the high-NO_x conditions.

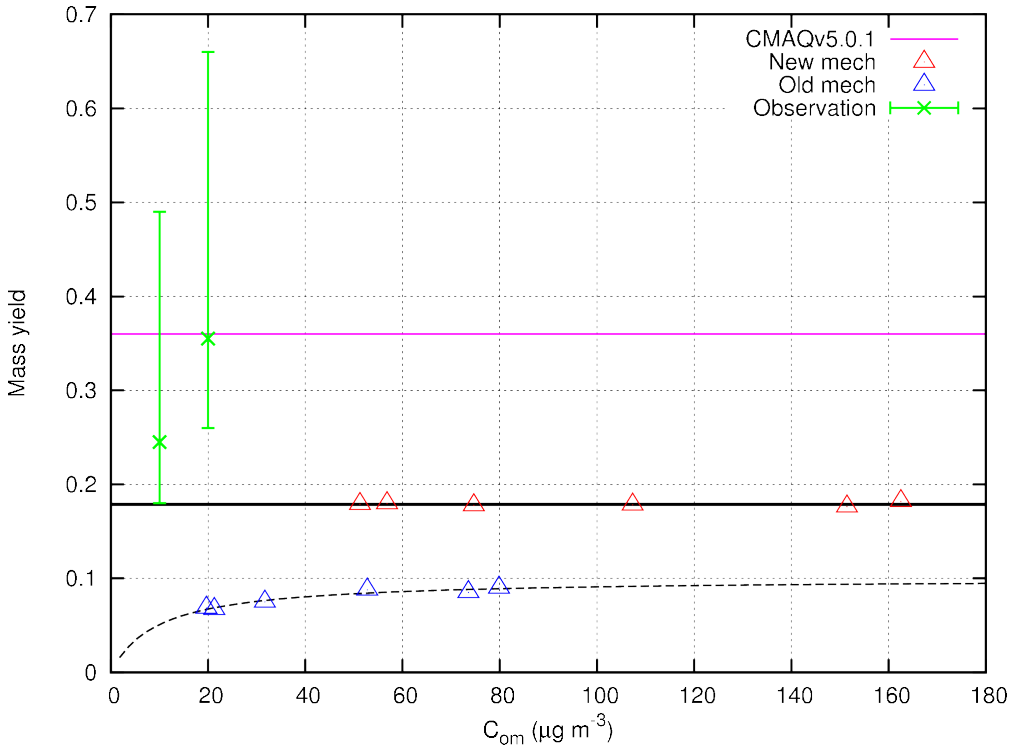

Figure S3 SOA yields under low-NO_x conditions used in the original CMAQ model (pink line) and those derived based on the photochemical box model simulations using the original MCM3.2 (Old mech) and the modified MCM3.2 mechanism with a higher branching ratio for the o-cresol pathway (New mech). Triangles show the yields at the end of each simulation. The green error bars show the minimum, maximum and mean SOA yields measured by Hildebrandt et al. at C_{om} = 10 and 20 μg m^{-3}.

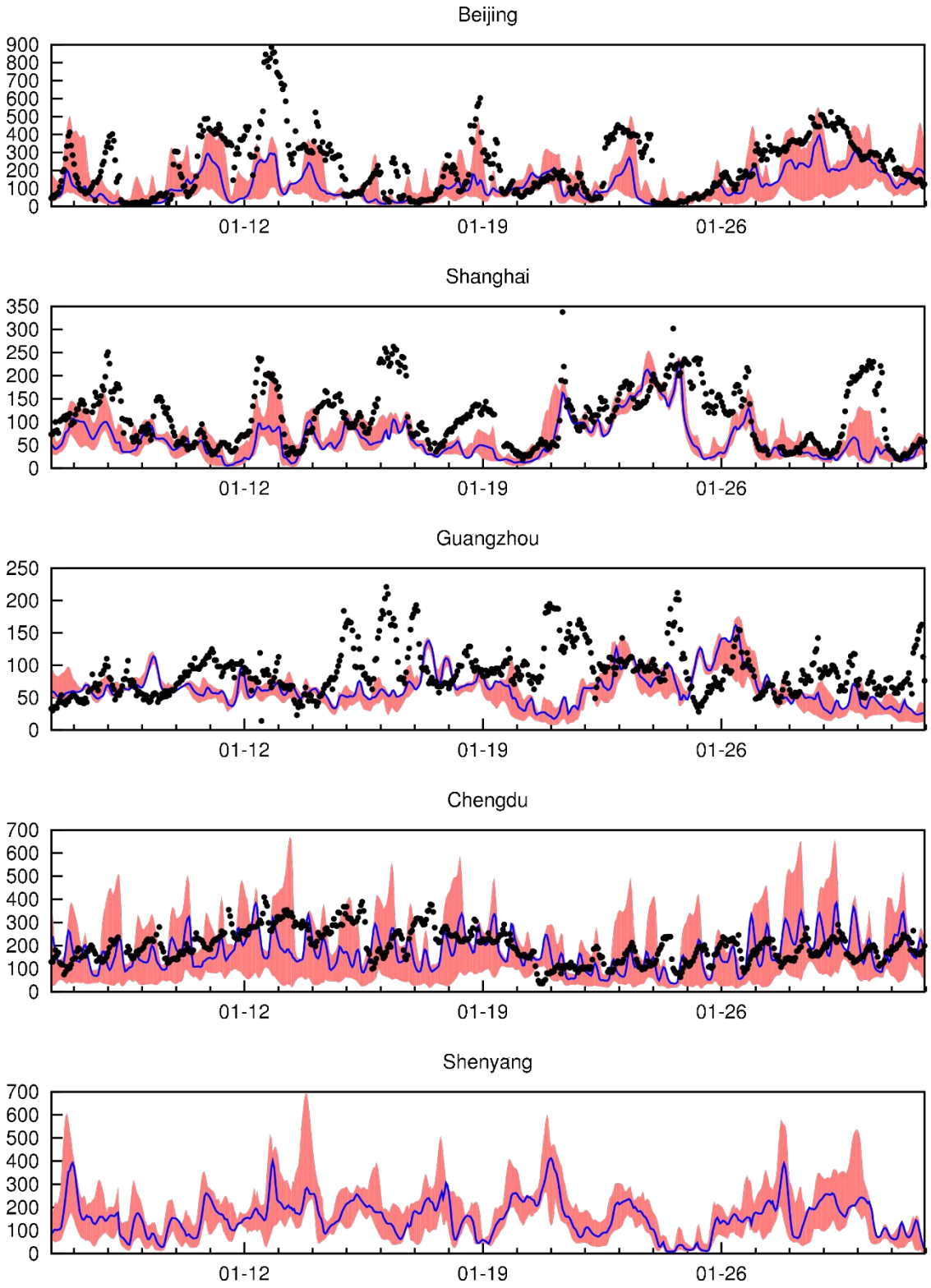

Figure S4. Predicted (blue line) and observed (black dots) hourly $PM_{2.5}$ concentrations in 5 Chinese cities in January 2013. The shaded areas represent the range of concentrations within the 9 grid cells (3x3) with the urban center in the middle. Units are μg m^{-3}.

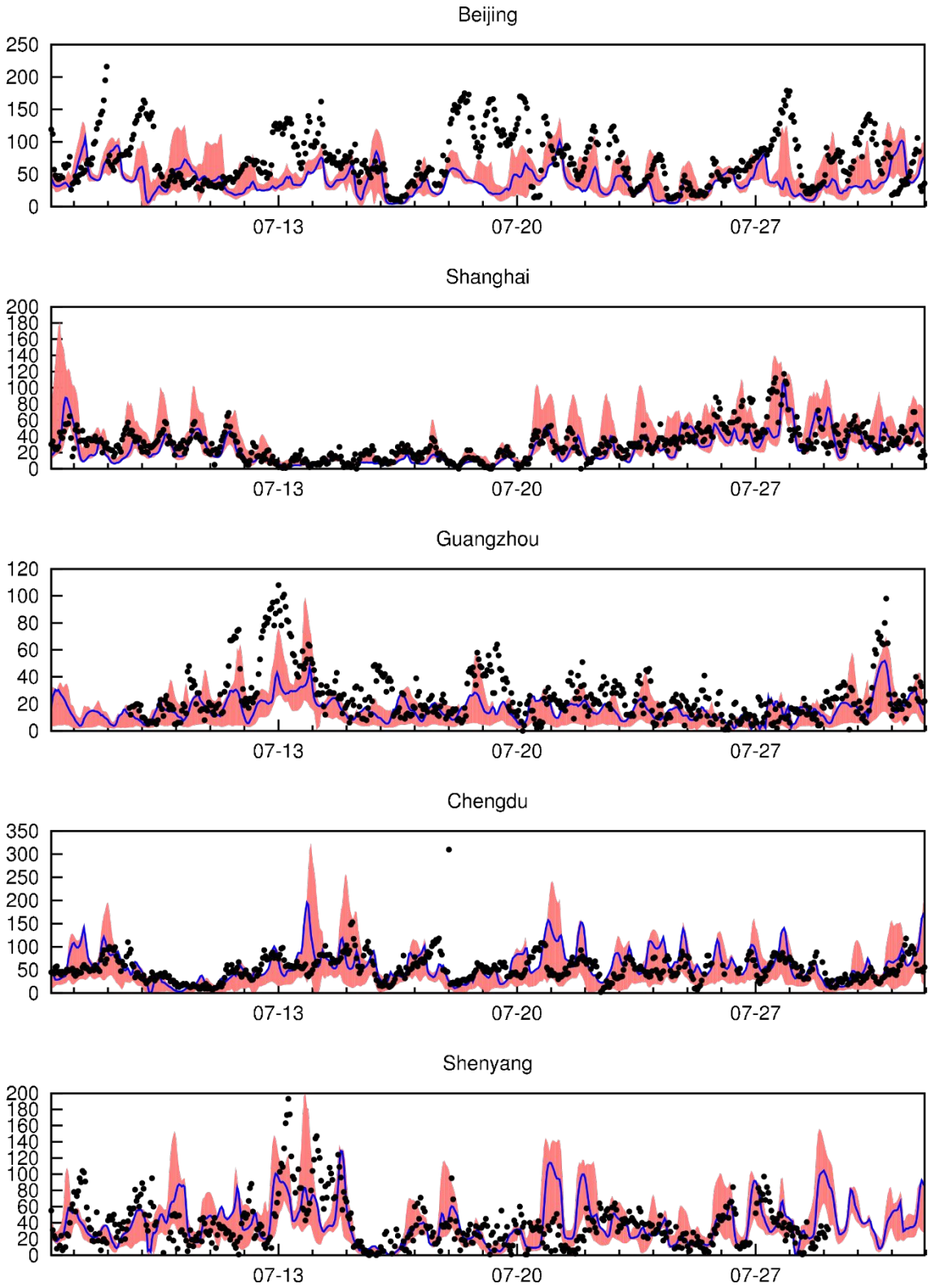

Figure S5. Predicted (blue line) and observed (black dots) hourly $PM_{2.5}$ concentrations in 5 Chinese cities in July 2013. The shaded areas represent the range of concentrations within the 9 grid cells (3x3) with the urban center in the middle. Units are μg m^{-3}.

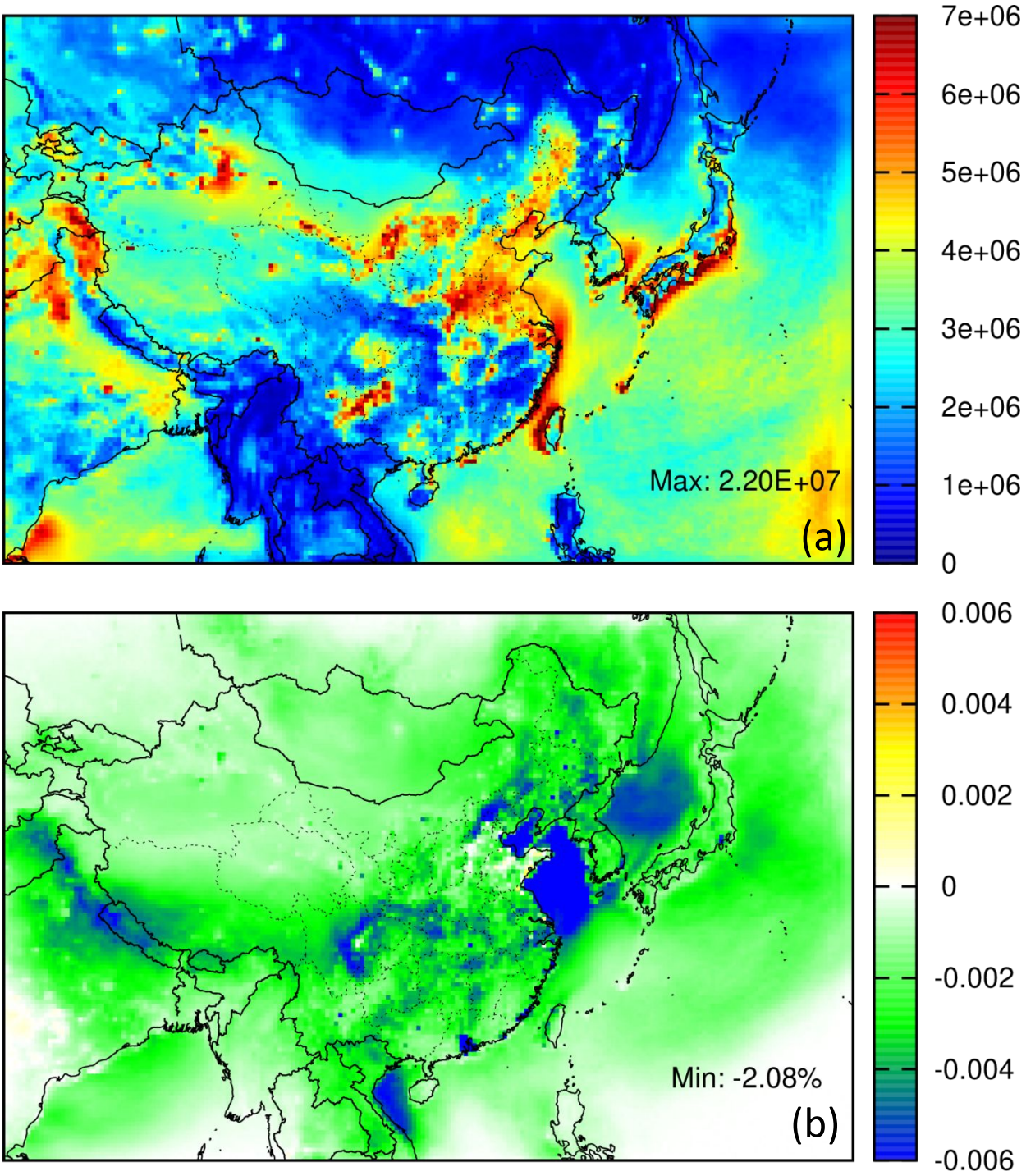

Figure S6. Monthly average OH radical concentrations (molecules cm^{-3}) from Case C1 for July 2013 (a), and the relative difference (Case C1-C0)/C0 (b).

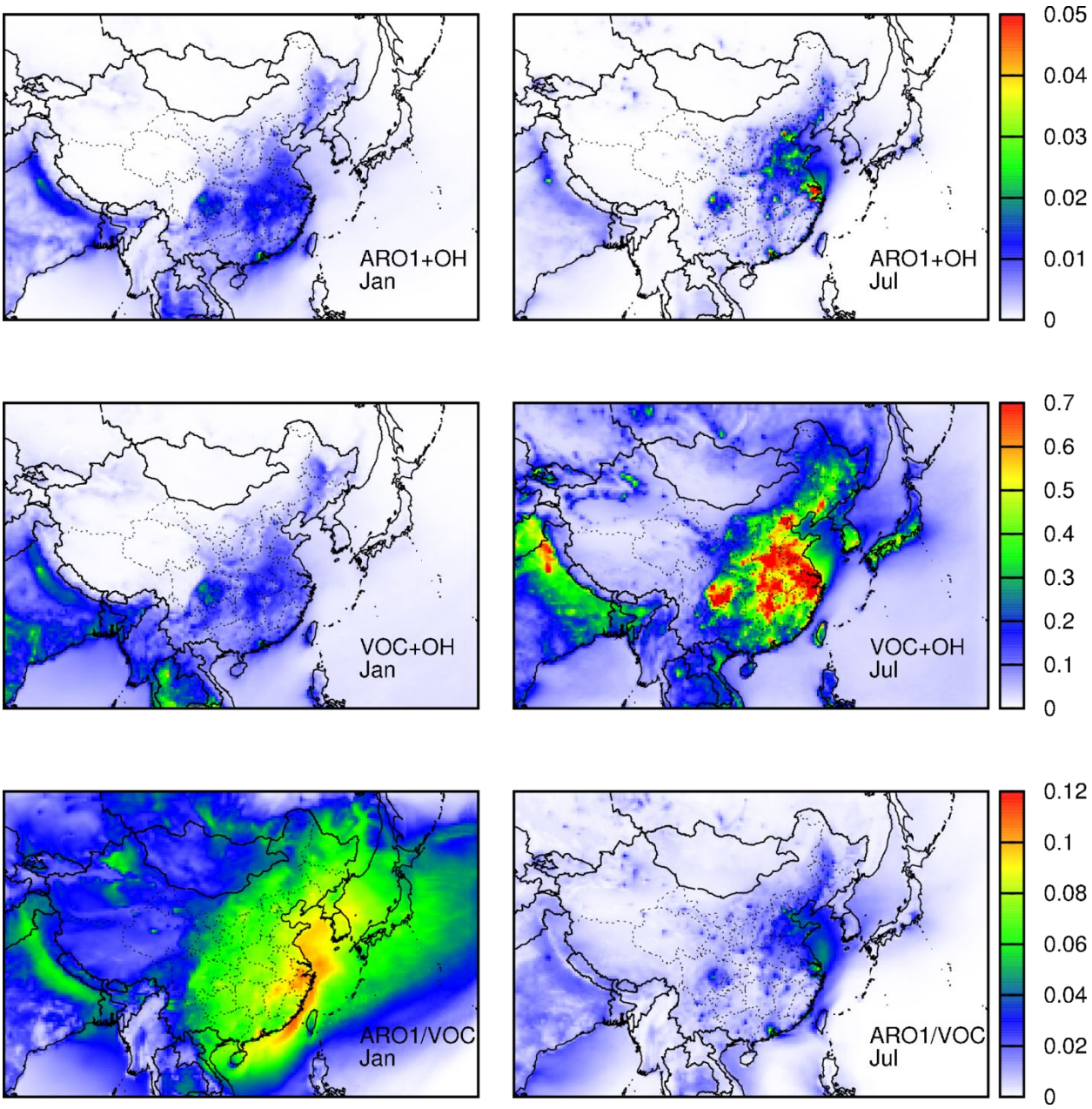

Figure S7. The amount of ARO1 and VOCs reacted with OH radical in one hour (ppb hr^{-1}) averaged for the entire month of January and July, and the fractional contribution of ARO1 in OH consumption by the VOCs.

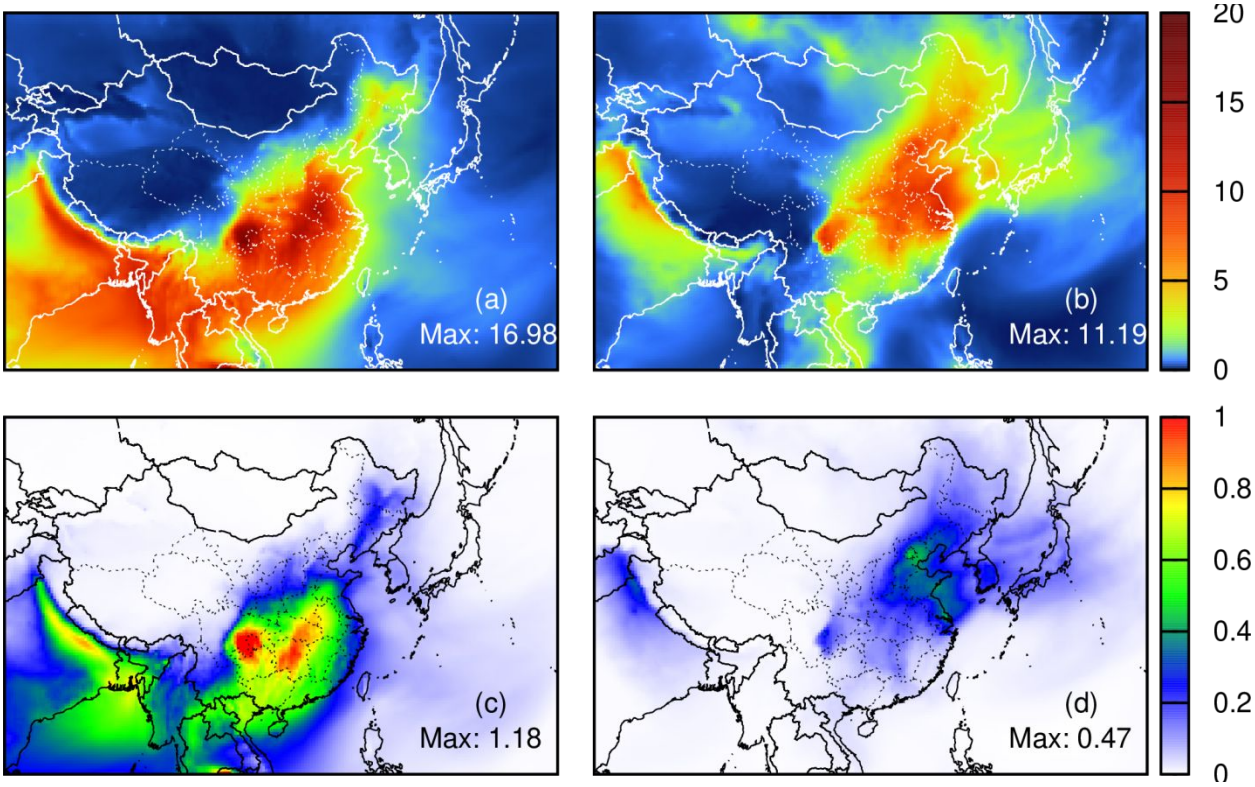

Figure S8. Predicted monthly average total SOA for January 2013 (a) and July 2013 (b) from Case C1, and the increase in total SOA (Case C1- Case C0) for January (c) and July 2013 (d). Units are μg m^{-3}.

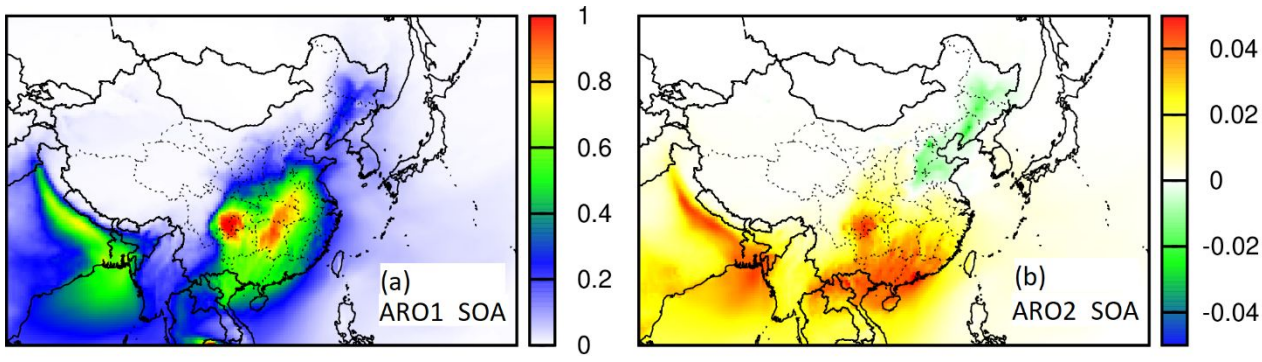

Figure S9. Increase in total SOA from (a) ARO1 and (b) ARO2 in January 2013 (Case C1 – Case C0). Units are μg m^{-3}.

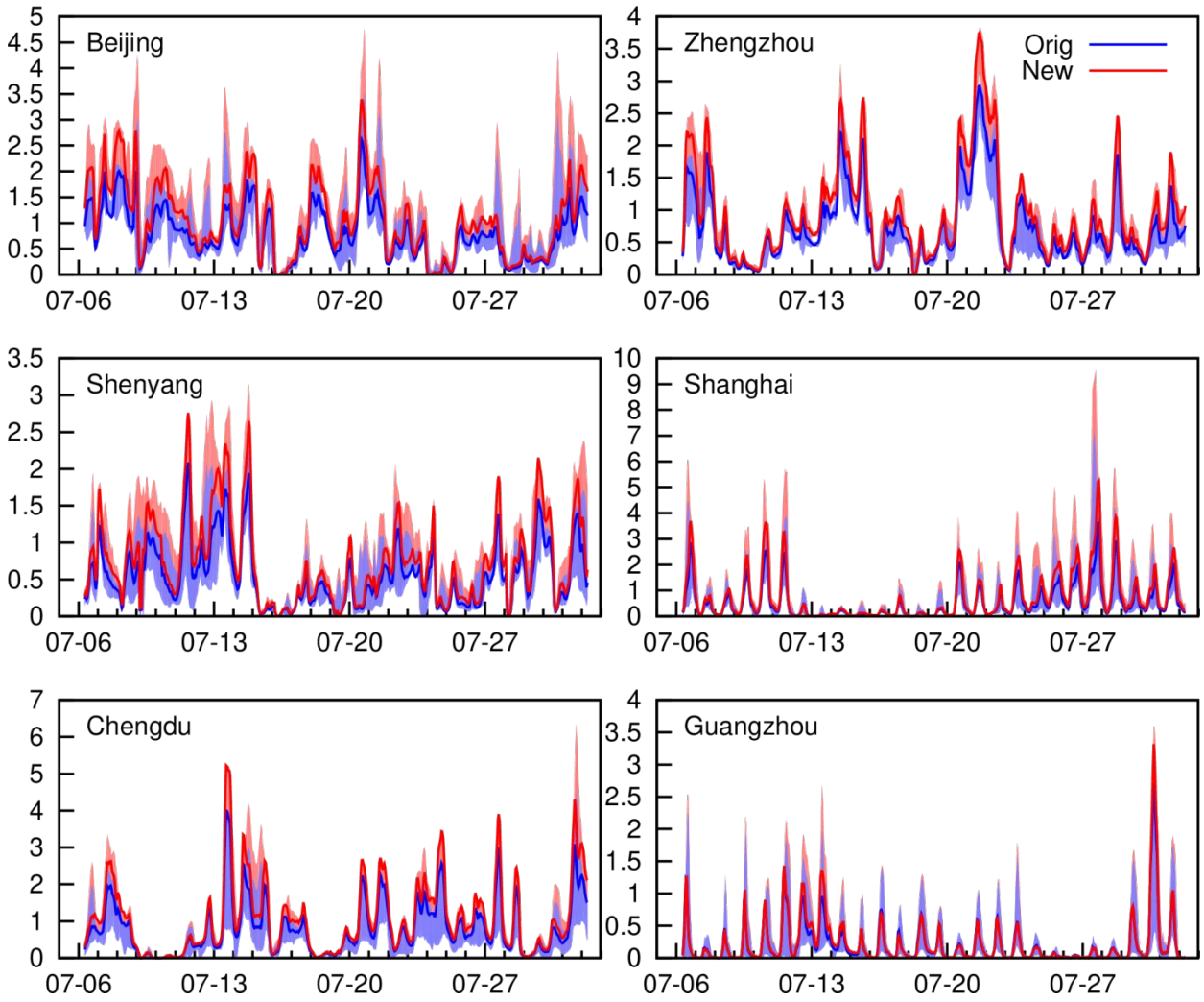

Figure S10. Predicted hourly concentrations of ARO1 SOA in several urban areas for July 2013 using the original and modified SOA yields. Units are μg m^{-3}. Shaded area represents the range of concentrations within the 3×3 grids with the urban center in the center grid. The solid lines are the average concentrations in the 3×3 grids.

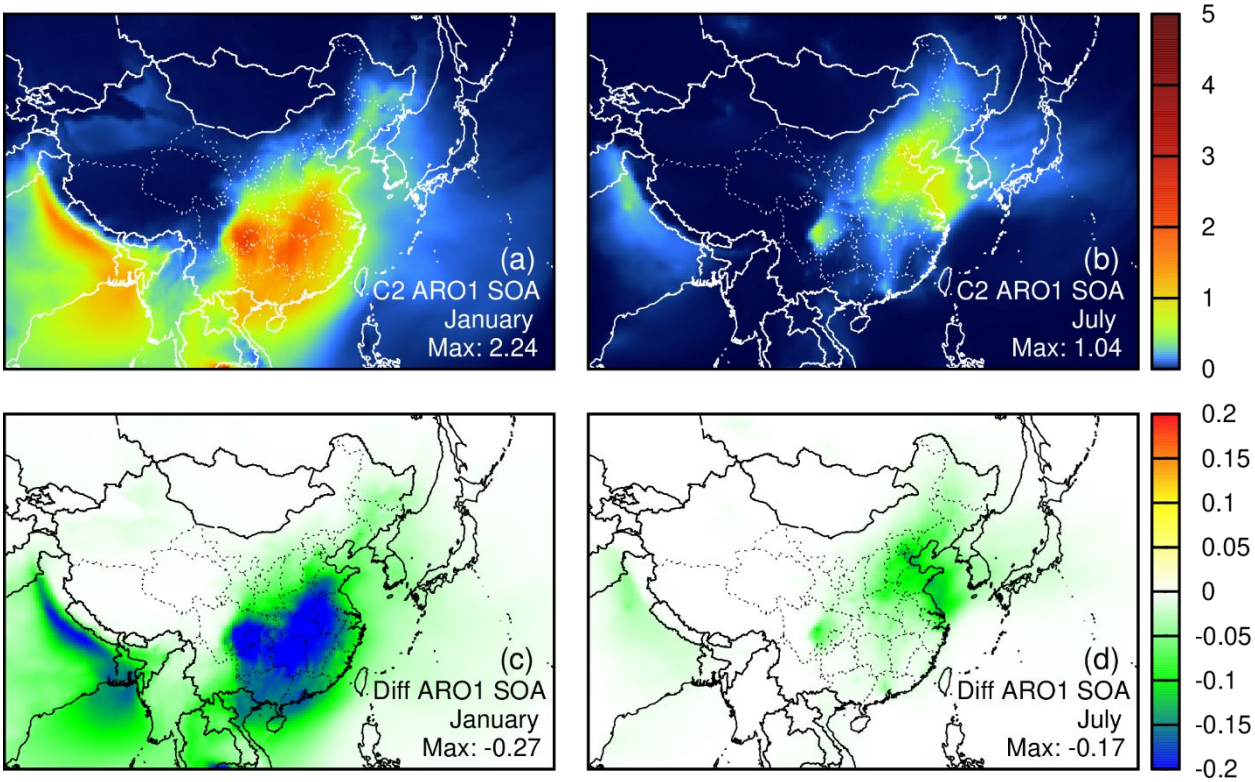

Figure S11. Predicted monthly average ARO1 SOA (Case C2) in January (a) and July (b) 2013. The monthly average ARO1 SOA changes (Case C2 – Case C0) for January (c) and July (d) 2013. Units are μg m^{-3}.

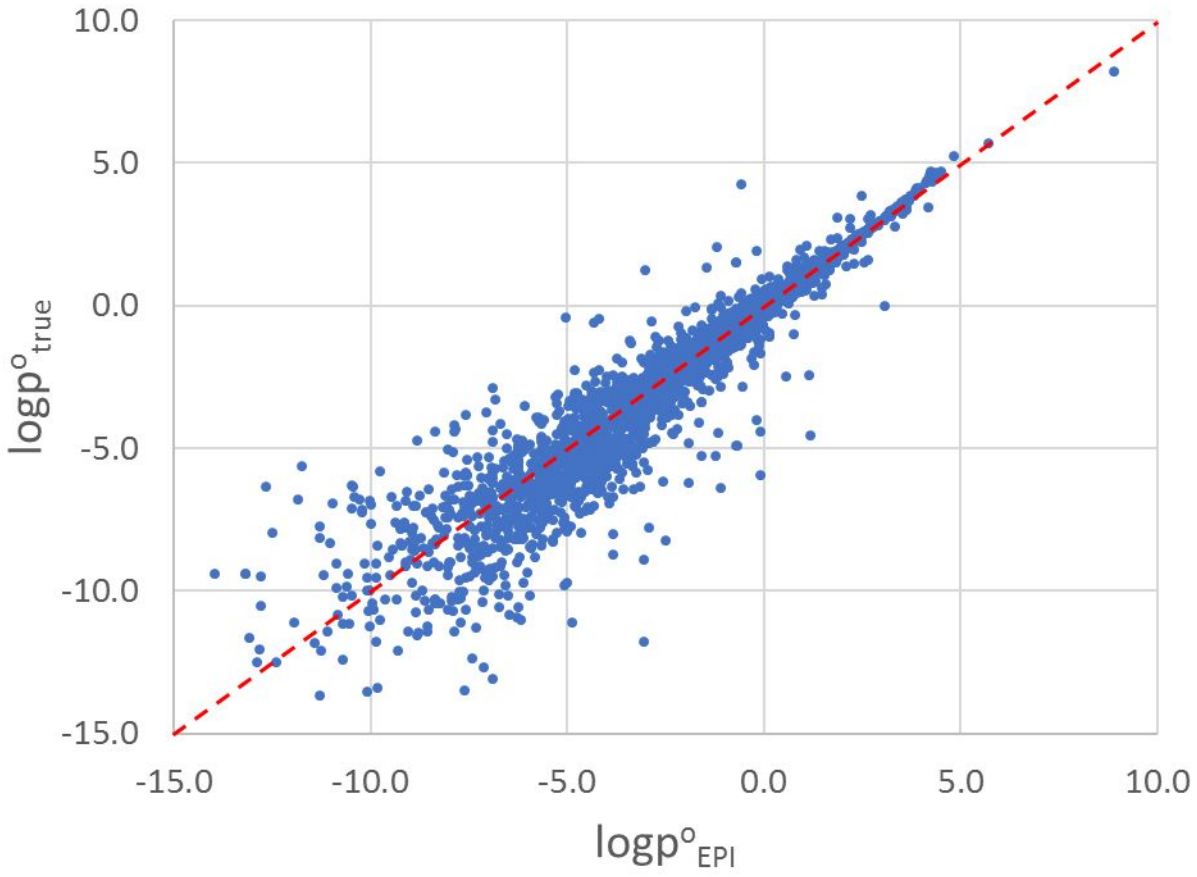

92

93 Figure S12. Predicted and experimental saturation vapor pressure for 3707 reference compounds
94 in the EPI suite database.

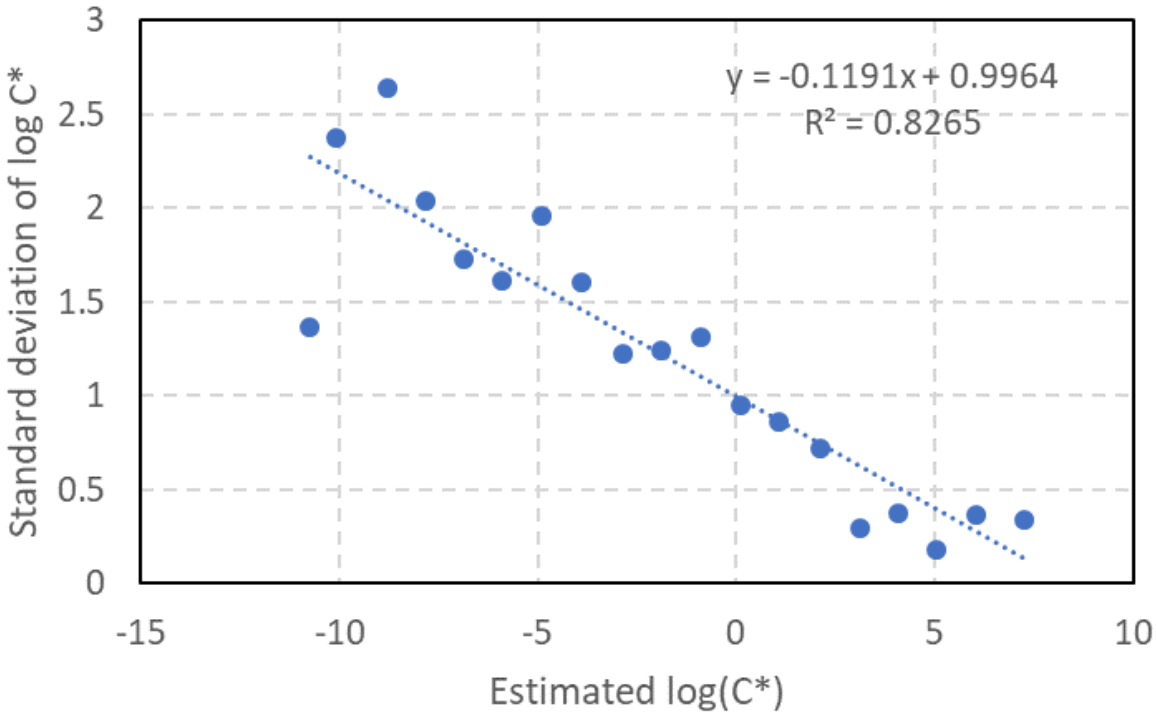

Figure S13. Standard deviation of estimated C^* as a function of C^*_{EPI}.

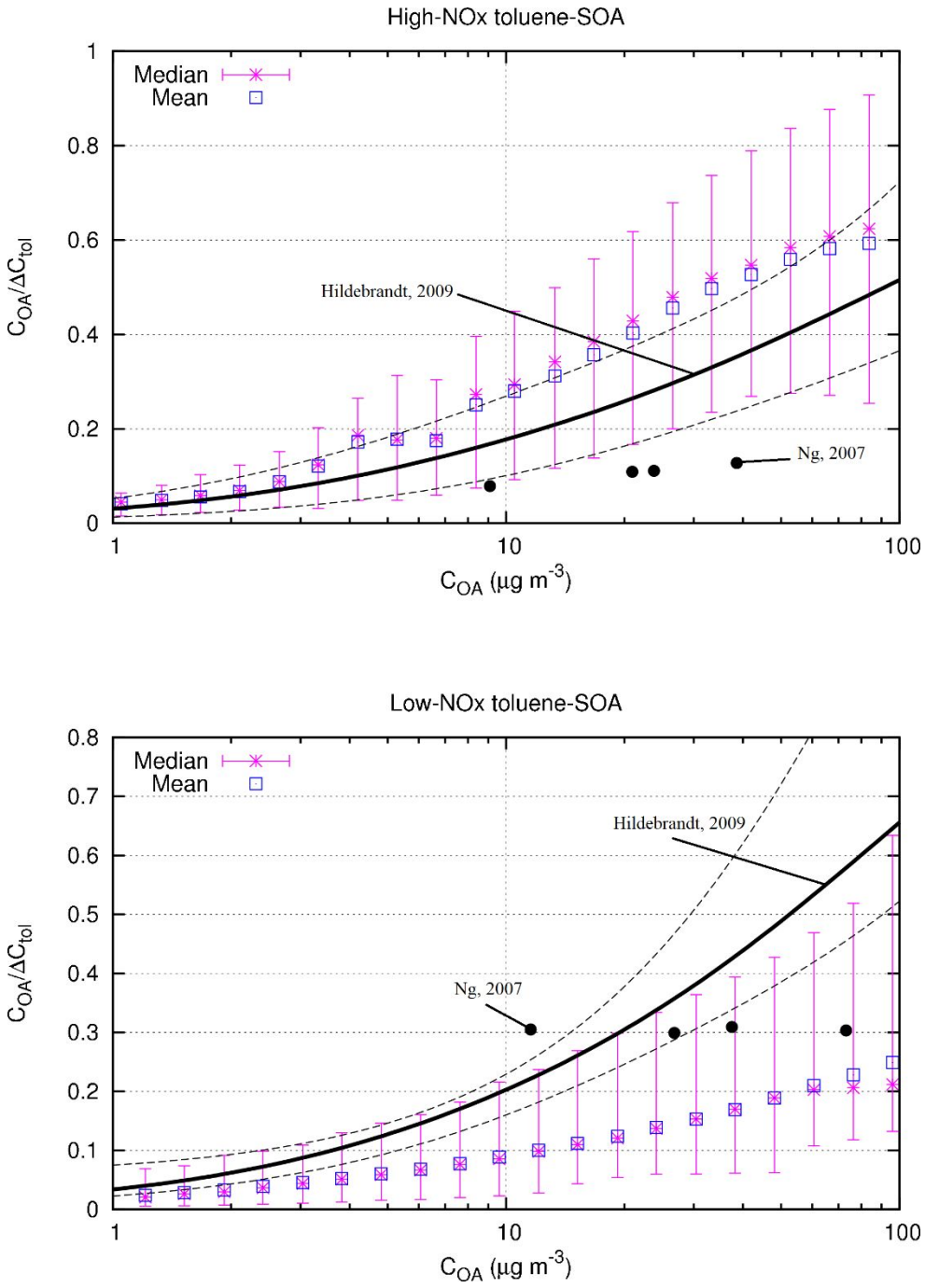

Figure S14. Uncertainty in the predicted SOA yields using the MCM mechanism due to uncertainty in the saturation vapor pressure of the semi-volatile products. The error bars are standard deviations calculated using 100 Monte Carlo simulations with randomly perturbed saturation vapor pressures. The dashed lines show the range of the SOA yield based on the experimental data (based on Figure 10 in Hildebrandt et al.[8])

Section S1. NO_2 photolysis rate in the MCM box model

NO_2 photolysis rate in the chamber experiments ($J_{NO_2,chamber}$) is subscribed in the simulation. Since the detailed spectrum of black lights in the chamber experiments are not reported, the photolysis rate of other reactions in the chamber ($J_{other,chamber}$) are calculated by adjusting the clear sky photolysis rate using the following equation,

$$J_{other,chamber} = \frac{J_{other,clear}}{J_{NO_2,clear}} J_{NO_2,chamber} \quad \text{(S1)}$$

Solar spectrum is used to calculate the clear sky photolysis rates.

In the H_2O_2 experiments, the photolysis rate of H_2O_2 is also calculated using the above equation, with $J_{NO_2,chamber}$ taken to be the same as the one determined in the high-NO_x experiments because they are performed in the same chambers with the same light source.

The zero solar zenith angle (θ_s) used in the calculation is chosen without a specific reason, as we assume that $\frac{J_{other,clear}}{J_{NO_2,clear}}$ is not a strong function of solar zenith angle (see Table S6below). The potential error in the estimation of the HNO_2 photolysis rate using the above equation at other solar zenith angles, when the ratio $\frac{J_{o,clear}}{J_{NO_2,clear}}$ is determined using a solar zenith angle of 0, is also shown in Table S6.

Table S6 Clear sky photolysis of NO_2 and HNO_2 at different solar zenith angles.

θ_s(°)	J_{NO_2} (min^{-1})	J_{HNO_2} (min^{-1})	J_{HNO_2}/J_{NO_2}	$J_{HNO_2,est}$*	Error^
0	0.656	0.107	0.163	0.107	0.0%
10	0.650	0.106	0.163	0.106	0.0%
20	0.632	0.103	0.163	0.103	0.3%
30	0.599	0.097	0.162	0.098	0.8%
40	0.548	0.088	0.161	0.089	1.5%
50	0.473	0.075	0.159	0.077	2.6%
60	0.370	0.058	0.156	0.060	4.4%
70	0.235	0.036	0.152	0.038	7.2%
80	0.091	0.014	0.149	0.015	9.2%
90	0.008	0.001	0.153	0.001	6.6%

* Estimated HNO_2 photolysis rates are based on the NO_2 photolysis rate at the specific θ_s and the constant rate of $J_{HNO_2}/J_{NO_2} = 0.163$ at $\theta_s = 0$.

^ Error is calculated as $(J_{HNO_2,est} - J_{HNO_2})/J_{HNO_2}$

As shown in Table S6, the relative error in the estimated J_{HNO_2} is less than 10% for solar zenith angles between 0 and 90 degrees. A better choice of solar zenith angle for our calculations would be ~80 degrees as it gives the NO_2 photolysis rate close to the reported value in the chamber, but it should not lead to significant differences in predicting SOA in the experiments.

The ratio $\frac{J_{other,clear}}{J_{NO_2,clear}}$ with black light might be different from those based on the solar spectrum. In another chamber study illuminated with black lights[9], the photolysis rate of NO_2 was determined from the photo-stationary relationship between NO_2, NO, and O_3, and the HNO_2 photolysis was calculated using the measured blacklight spectrum. J_{HNO_2}/J_{NO_2} was reported to be 0.145, close to the ratio of 0.161 used in our study. Furthermore, the modeled OH radical concentrations in the chamber experiments are close to the reported OH based on the decay of the precursor, further suggesting that the photolysis rates used in this study are reasonable.

Section S2. Full reactions of original, upper limit, and modified ARO1+OH used in the study

The original ARO1 + OH reaction in the SAPRC-11 mechanism is shown as the Reaction RS1, which is used in the simulation of Case C0.

ARO1 + OH = 0.089 RO2XC + 0.622 RO2C + 0.209 HO2 + 0.612 xHO2 + 0.089 zRNO3 + 0.14 yR6OOH + 0.007 xMEO2 + 0.049 xBALD + 0.064 xPROD2 + 0.003 xCCHO + 0.006 xRCHO + 0.135 CRES + 0.032 XYNL + 0.268 xGLY + 0.231 xMGLY + 0.255 xAFG1 + 0.244 xAFG2 + 0.567 yRAOOH + 0.084 OH + 0.084 AFG3 + 0.042 AFG5 (RS1)

The upper-limit ARO1 + OH reaction assuming the OH + ring reactions generate cresol (from toluene) and phenolic compounds (from other monoalkylbenzenes) only.

ARO1 + OH = 0.014 RO2XC + 0.099 RO2C + 0.887 HO2 + 0.065 xHO2 + 0.0015 zRNO3 + 0.14 yR6OOH + 0.049 xBALD + 0.064 xPROD2 + 0.717 CRES + 0.170 XYNL (RS2)

The modified ARO1 + OH reaction in the SAPRC-11 mechanism is shown as the Reaction RS3, which is used in the simulation of Case C1 and C2.

ARO1 + OH = 0.059 RO2XC + 0.415 RO2C + 0.477 HO2 + 0.396 xHO2 + 0.0727 zRNO3 + 0.14 yR6OOH + 0.0042 xMEO2 + 0.049 xBALD + 0.064 xPROD2 + 0.0018 xCCHO + 0.0036 xRCHO + 0.365 CRES + 0.087 XYNL + 0.162 xGLY + 0.140 xMGLY + 0.154 xAFG1 + 0.147 xAFG2 + 0.342 yRAOOH + 0.051 OH + 0.051 AFG3 + 0.025 AFG5 (RS3)

Section S3. Evaluation of the modified SAPRC-11 ARO1 mechanism on O_3 formation using smog chamber data

The SAPRC modeling program for chamber experiments was used to simulate 16 EPA smog chamber experiments, selected from the collection of chamber experiments used to evaluate the SAPRC mechanisms, to understand how the higher cresol branching ratio of toluene-OH initial oxidation changes the O_3 formation simulation in box models. The programs and the input data for the chamber experiments were downloaded from Dr. William P.L. Carter's SAPRC mechanism website (https://intra.engr.ucr.edu/~carter/SAPRC/SAPRCfiles.htm). The details of the selected experiments, including the toluene and NO_x initial concentrations and the smog chamber conditions, are shown in Table S7. Each of the smog chamber experiments lasted for 6-10 hours. For each chamber experiment, three cases were simulated, 1) with the original ARO1 mechanism in the lumped SAPRC-11, 2) with the modified ARO1 mechanism, as shown in Table 2, and 3) the explicit toluene mechanism in the detailed version of the SAPRC-11. The original ARO1 mechanism and the detailed toluene mechanism simulate the chamber data better as the SAPRC mechanism is optimized based on the chamber data. The modified ARO1 mechanism leads to slightly slower consumption of toluene and early formation of O_3 in the initial stage of the experiments. In addition, the O_3 concentrations at the end of the experiments are slightly lower than those based on the original mechanism, which agrees with the O_3 responses to the toluene-OH branching ratios modification. Figure S15 shows a representative O_3 time series in one chamber experiments, and the comparison of the final O_3 concentrations in these simulations against observations is shown in Figure S16. The lower O_3 formation with a higher yield for the cresol pathway has also been verified in MCM box model simulations.

Table S7 Selected smog chamber experiments used to test the modified SAPRC-11 toluene and ARO1 mechanisms.

Run ID	Initial Reactant Summary			Light Type	J_{NO2}	Avg. Temp	Running time	PM Wall Loss
	Test. VOC	VOC (ppm)	NO_x (ppb)		(min^{-1})	(K)	(min)	
EPA210A	TOLUENE	0.26	42	Arc light solar simulator	0.260	305	377	6.3E-03
EPA210B	TOLUENE	0.26	93	Arc light solar simulator	0.260	305	377	5.4E-03
EPA443A	TOLUENE	0.17	31	Arc light solar simulator	0.260	304	364	3.3E-03
EPA443B	TOLUENE	0.36	99	Arc light solar simulator	0.260	304	364	3.3E-03
EPA289B	TOLUENE	0.22	25	Blacklights	0.165	301	492	2.9E-03
EPA1098A	TOLUENE	0.08	16	Blacklights	0.131	298	583	5.0E-03
EPA1098B	TOLUENE	0.08	30	Blacklights	0.131	298	360	3.5E-03
EPA1099B	TOLUENE	0.04	10	Blacklights	0.131	298	487	3.9E-03
EPA1101A	TOLUENE	0.08	19	Blacklights	0.401	300	491	5.5E-03
EPA1101B	TOLUENE	0.08	9	Blacklights	0.401	300	360	4.5E-03
EPA1102A	TOLUENE	0.08	43	Blacklights	0.401	300	474	6.0E-03
EPA1102B	TOLUENE	0.08	32	Blacklights	0.401	300	474	4.5E-03
EPA1106A	TOLUENE	0.03	20	Blacklights	0.401	300	630	6.2E-03
EPA1106B	TOLUENE	0.03	11	Blacklights	0.401	300	630	6.0E-03
EPA1107A	TOLUENE	0.04	40	Blacklights	0.401	300	595	5.7E-03
EPA1107B	TOLUENE	0.04	30	Blacklights	0.401	300	595	6.4E-03

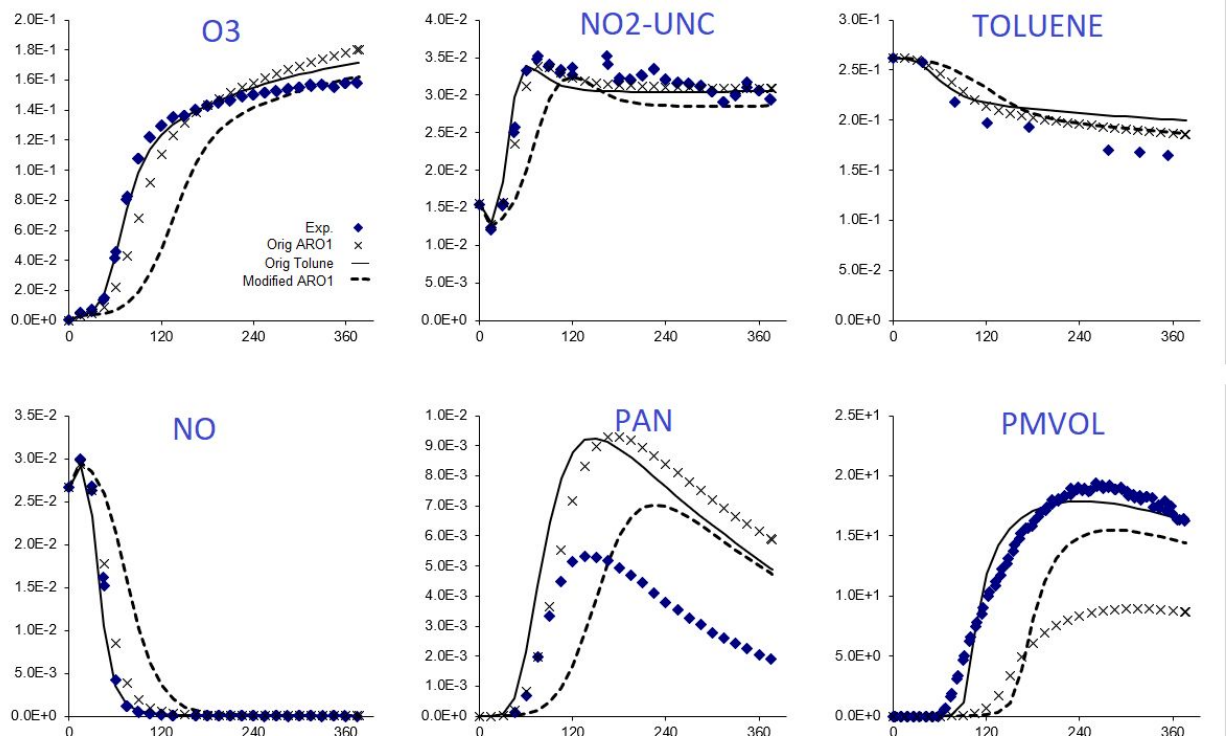

Figure S15. Time series of O_3, NO_2 (NO2-UNC), toluene (TOLUENE), NO, PAN and PM volume in the smog chamber experiments using the original lumped ARO1 mechanism, the original toluene mechanism and the modified ARO1 mechanism for the chamber experiment EPA210A.

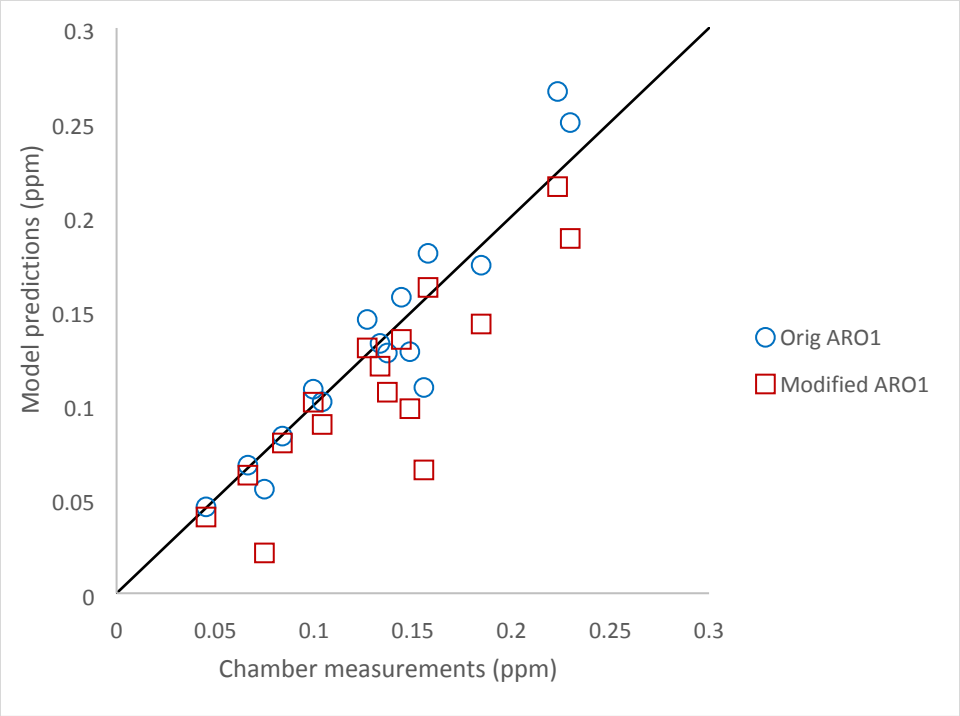

Figure S16. Comparison of the final O_3 concentrations in the chamber experiments simulated using the original ARO1 and modified ARO1 mechanisms with observations.

Section S4. Evaluation of the MCM-based box model in simulating other chamber experiments

We obtained three sets of chamber data reported by Ng et al.[10], including the time series of toluene and particle and vapor wall-loss corrected SOA, from Dr. Shantanu Jathar of Colorado State (with consent from Sally Ng). Two datasets (Cases 1 and 3) are for high-NO_x conditions, and one dataset (Case 2) is for low-NOx conditions. HONO was used as the OH source for Cases 1 and 3, and NO and NO_2 were added to ensure an initial NOx concentration of 1 ppm. H_2O_2 was used as the OH source for Case 2 with an initial concentration of 5 ppm. The OH concentrations in the chamber experiments were not directly measured. We estimated OH concentrations by assuming decay of toluene is caused by OH only and using $k_{tol+OH}=5.63\times10^{-12}$ cm^3 $molecules^{-1}$ s^{-1} at 25 ℃[10]. The photolysis rate of NO_2 was estimated to be 0.45 min^{-1} for all three cases, which correctly predicts the decay of toluene and the OH concentration in the chamber (see Figure S17).

Under low NO_x conditions, the model predicted SOA yields with both the original (low cresol pathway) and new (high cresol pathway) mechanisms were lower than the chamber measurements. This is consistent with the results obtained when simulating the low-NOx chamber experiments from Hildebrandt et al.[8] Under high NO_x conditions, the measured SOA yields in Ng et al. were lower (~0.1 at OM = 20 μg m^{-3}) than those in Hildebrandt et al.[8] (0.15-0.45 at OM = 20 μg m^{-3}). The differences in the predicted SOA yields from the original and the modified mechanism are small. The new mechanism still predicted higher SOA yields, as reported in the original manuscript when simulating Hildebrandt et al.'s data, and has a slightly closer agreement with the vapor wall-loss corrected SOA yields.

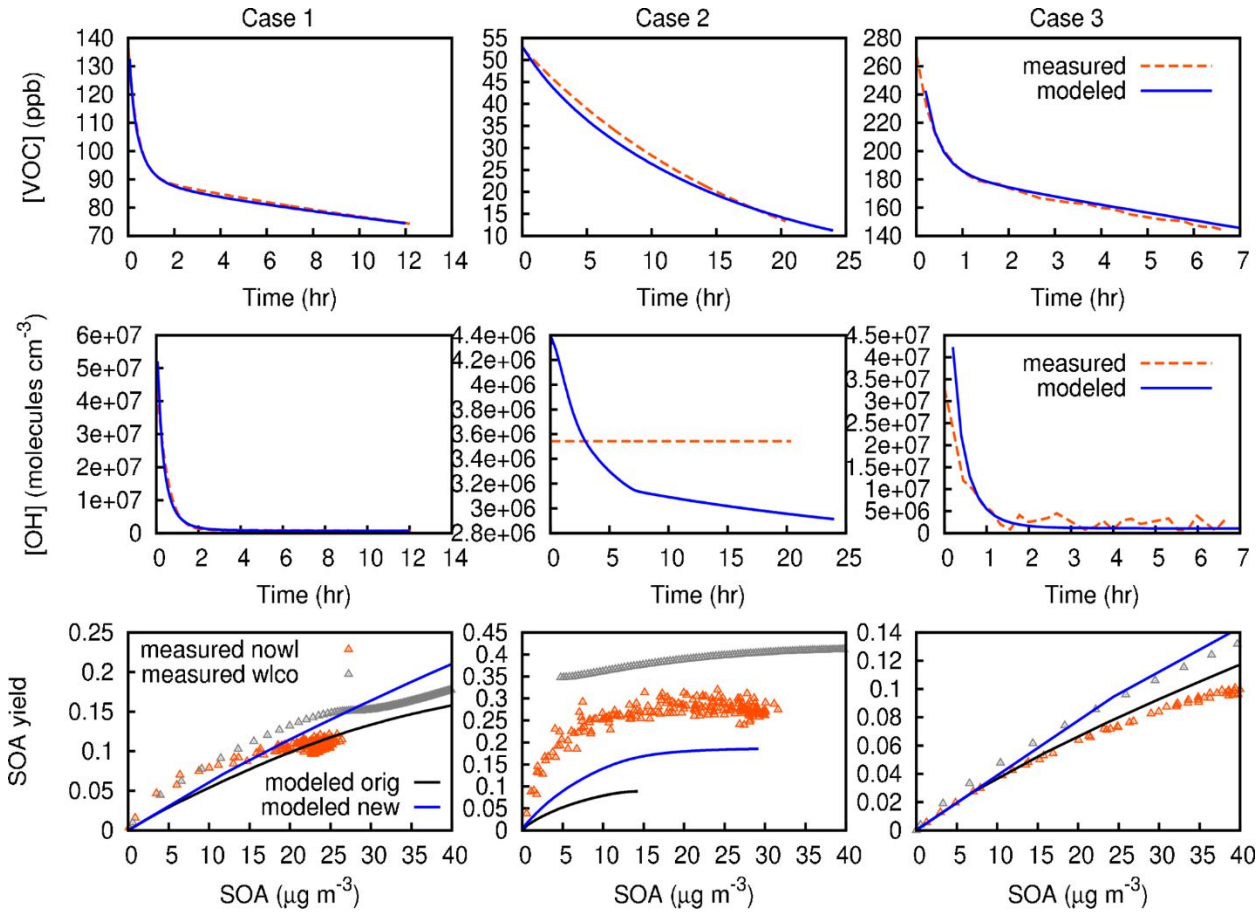

Figure S17. Comparison predicted and MCM modeled time series of toluene and OH concentrations, and SOA yields. "measured nowl" is the SOA yields without vapor wall-loss correction. "measured wlco" is SOA yields calculated based on vapor wall-loss corrected SOA concentrations.

References

1. Li, J.; Xie, S. D.; Zeng, L. M.; Li, L. Y.; Li, Y. Q.; Wu, R. R., Characterization of ambient volatile organic compounds and their sources in Beijing, before, during, and after Asia-Pacific Economic Cooperation China 2014. *Atmos. Chem. Phys.* **2015,** *15*, (14), 7945-7959.
2. Song, M.; Tan, Q.; Feng, M.; Qu, Y.; Liu, X.; An, J.; Zhang, Y., Source Apportionment and Secondary Transformation of Atmospheric Nonmethane Hydrocarbons in Chengdu, Southwest China. *Journal of Geophysical Research: Atmospheres* **2018,** *123*, (17), 9741-9763.
3. Han, D.; Wang, Z.; Cheng, J.; Wang, Q.; Chen, X.; Wang, H., Volatile organic compounds (VOCs) during non-haze and haze days in Shanghai: characterization and secondary organic aerosol (SOA) formation. *Environmental Science and Pollution Research* **2017,** *24*, (22), 18619-18629.
4. Zhang, Y.; Wang, X.; Barletta, B.; Simpson, I. J.; Blake, D. R.; Fu, X.; Zhang, Z.; He, Q.; Liu, T.; Zhao, X.; Ding, X., Source attributions of hazardous aromatic hydrocarbons in urban, suburban and rural areas in the Pearl River Delta (PRD) region. *Journal of Hazardous Materials* **2013,** *250-251*, 403-411.
5. Xia, L.; Cai, C.; Zhu, B.; An, J.; Li, Y.; Li, Y., Source apportionment of VOCs in a suburb of Nanjing, China, in autumn and winter. *Journal of Atmospheric Chemistry* **2014,** *71*, (3), 175-193.
6. Hu, J.; Wang, P.; Ying, Q.; Zhang, H.; Chen, J.; Ge, X.; Li, X.; Jiang, J.; Wang, S.; Zhang, J.; Zhao, Y.; Zhang, Y., Modeling biogenic and anthropogenic secondary organic aerosol in China. *Atmos. Chem. Phys.* **2017,** *17*, (1), 77-92.
7. Yun, H.; Wang, W.; Wang, T.; Xia, M.; Yu, C.; Wang, Z.; Poon, S. C.; Yue, D.; Zhou, Y., Nitrate formation from heterogeneous uptake of dinitrogen pentoxide during a severe winter haze in southern China. *Atmospheric chemistry and physics* **2018**.
8. Hildebrandt, L.; Donahue, N. M.; Pandis, S. N., High formation of secondary organic aerosol from the photo-oxidation of toluene. *Atmospheric Chemistry & Physics Discussions* **2009,** *9*, (1).
9. Jia, L.; Xu, Y.; Ge, M.; Du, L.; Zhuang, G., Smog chamber studies of ozone formation potentials for isopentane. *Chinese Science Bulletin* **2009,** *54*, (24), 4624-4632.
10. Ng, N.; Kroll, J.; Chan, A.; Chhabra, P.; Flagan, R.; Seinfeld, J., Secondary organic aerosol formation from m-xylene, toluene, and benzene. **2007**.